

Mutual synchronization and clustering in randomly coupled chaotic dynamical networks

Susanna C. Manrubia and Alexander S. Mikhailov

Fritz-Haber-Institut der Max-Planck-Gesellschaft, Faradayweg 4-6, 14195 Berlin, Germany

We introduce and study systems of randomly coupled maps (RCM) where the relevant parameter is the degree of connectivity in the system. Global (almost-) synchronized states are found (equivalent to the synchronization observed in globally coupled maps) until a certain critical threshold for the connectivity is reached. We further show that not only the average connectivity, but also the architecture of the couplings is responsible for the cluster structure observed. We analyse the different phases of the system and use various correlation measures in order to detect ordered non-synchronized states. Finally, it is shown that the system displays a dynamical hierarchical clustering which allows the definition of emerging graphs.

PACS number(s): 05.45.+b, 05.20.-y, 05.90.+m

I. INTRODUCTION

Since their introduction in 1989 [1,2], globally coupled maps (GCM) have turned out to be a paradigmatic example in the study of the emergent behavior of complex systems as diverse as ecological networks, the immune system, or neural and cellular networks. It has been shown that mutual synchronization of chaotic oscillations is a robust property displayed by GCM [2,3]. Effects of mutual synchronization are also known for coupled chaotic oscillators with continuous time [4]. A recent study [5] of large globally coupled populations formed by chaotic Rossler oscillators has revealed that mutual synchronization and dynamical clustering in these systems are similar to the respective behaviour found in GCM. Another well investigated class of self-synchronizing systems represents lattices of locally (e.g., diffusively) coupled oscillators [6]. Moreover, oscillator systems with both local and global coupling between elements have also been discussed [7]. A common property of GCM and other above-mentioned systems is their architectural symmetry: The pattern of connections of any individual element is identical. This internal symmetry is preserved in the fully synchronized dynamical states and spontaneously broken when dynamical clustering takes place.

The architecture of dynamical networks found in real ecological or other systems would rarely be so symmetric. Even in the situations with high connectivity, when the links can extend to many distant elements, the graph of connections may have a complex topology. The question is therefore whether and in what form mutual synchronization and dynamical clustering can persist in such complexly connected networks, lacking a structural symmetry. In this direction, among the few cases already explored we can mention a layered system of identical random neural networks with partial (though regular) connectivity among layers [8], coupled lattice maps with connections extending further than to nearest neighbors [9], as well as coupled lattice oscillators in 2-D with different coupling schemes [10] or a model ecosystem with

partial connectivity [11]. More recently, ensembles of nonlinear oscillators [12] and GCM [13] with random interactions and variable symmetry (still globally coupled) have also been analyzed.

The analysis of systems formed by few coupled chaotic elements complements the previous approach and has provided a better understanding of the collective behaviour displayed by large ensembles of regularly connected chaotic oscillators. The stability of the synchronous state can be in this case easily quantified by means of the transverse Lyapunov exponent λ_\perp , which changes sign in a blow-out bifurcation [14] and makes the synchronous state unstable. Near the bifurcation, on-off intermittency [15] and riddled basins of attraction [16] are observed. Much attention has been devoted to the dynamical properties of systems formed by two coupled, identical chaotic elements [17]. The synchronization properties of two coupled logistic maps have been extensively investigated [18].

As the next step towards understanding the synchronization phenomena in complex networks, one can consider systems formed by a large number of identical dynamical elements that are connected by identical symmetrical links but where the pattern of connections between elements is random. This is the starting point of our paper. In the following sections we introduce and analyse what we have termed Randomly Coupled Maps (RCM), that is, networks of chaotic maps connected (symmetrically) at random where the relevant parameter is the average connectivity in the system.

Our main result is that mutual synchronization and dynamical clustering are possible in RCM even when a significant fraction (up to 40-45%) of all potential connections is absent. However, the synchronization and clustering phenomena in these systems are different in certain aspects from what is known for GCM. Exact synchronization and the formation of identical dynamical states of the elements are not found here. Instead, either one or several compact clouds (fuzzy clusters) are formed. These fuzzy clusters are dynamical objects which split into subclusters or join other groups of elements. Such

dynamical hierarchy of clusters is almost never completely fixed in time. A closely related effect is that the asymptotic dynamical behavior in RCM is never sensitive to the initial conditions. However, the architecture of a particular network may bias the synchronization process and make certain cluster distributions more favourable. The role of the network is particularly evident when the system is small, ($N \rightarrow 0(1)$): In this case, the synchronization properties of the system are strongly dependent on the particular architecture, and graphs with the same connectivity might have very different collective behavior. We will show that only in the thermodynamic limit do the synchronization properties of RCM become equivalent to the globally coupled case.

In the next Section we introduce the model and describe its dynamical behavior. In Section III the synchronous and the partially ordered phases of the system are quantitatively characterized by computing properties such as the mutual information and two order parameters of the synchronization transition. A more detailed statistical investigation is then performed in Section IV where distributions over pair distances are constructed. Section V is devoted to the analysis of the emergent cluster structure in partially condensed phases. A complement to the latter section is the Appendix, where an example of a small system with varying network architectures is considered. Finally, in Section VI we discuss our results, come to the conclusions and outline future extensions of this study.

II. THE RANDOMLY COUPLED MAPS

We begin by exactly defining what we have termed Randomly Coupled Maps. Instead of a globally coupled system, this will be a network of connections characterized through a random matrix T_{ij} , the elements of which are either 0 (when a connection between maps i and j is absent) or 1. In our analysis, we assume that the matrix is symmetric, i.e. $T_{ij} = T_{ji}$, and all diagonal elements are set to 0 ($T_{ii} = 0$). An important property of such random networks is their average connectivity

$$\bar{c} = \frac{1}{N(N-1)} \sum_{i,j=1}^N T_{ij} \quad (1)$$

Hence, each element will be on the average connected to $(N-1)\bar{c}$ elements in the system. If $\bar{c} = 1$, the system is globally coupled and our system reduces to this known system.

The collective dynamics of RCM is defined as

$$x^i(t+1) = \Theta \left(1 - \frac{1}{N-1} \sum_{j=1}^N T_{ij} A f(x^j(t)) + \frac{1}{N-1} \sum_{j=1}^N T_{ij} f(x^j(t)) \right) \quad (2)$$

where Θ specifies the strength of the coupling and $f(x)$ is the individual map. This collective dynamics can thus be understood as involving diffusion on a graph: Each node in the random graph diffuses a certain fraction of material (its state) to the elements to which it is connected, and receives a comparable influence from them. The intensity of coupling between the network elements is specified by the parameter Θ (we have the constraint $\Theta < 1$). Nevertheless, the combination $\Theta = \bar{c}$, which can be interpreted as a diffusion coefficient, plays an important role. Note that in the limit $N \rightarrow \infty$ all RCM with a given connectivity become statistically identical. Indeed, in this limit each element will have the same number $N\bar{c}$ of connections, although still it is linked only to a randomly chosen subpopulation. If the mean-field approximation holds, the behavior of this system would therefore be equivalent to the behavior of a GCM with coupling intensity \bar{c} .

In this paper we investigate differences in the behavior of GCM and RCM with large, but finite numbers of elements. We work with the logistic map $f(x) = 1 - ax^2$ and use values of a such that the dynamics of a single map is chaotic. Our numerical simulations are performed for graphs with sizes up to $N = 2048$ elements and with connectivities in the interval $0.5 < \bar{c} < 1$. Such graphs have been randomly generated by independently choosing every possible connection with the same fixed probability. We have checked that thus generated graphs remained fully connected, i.e. they could not be further separated into two disconnected parts.

Considering that we wish to compare the behaviour of RCM with that of GCM, it is of interest to begin by briefly recalling the dynamic behaviour of GCM when the coupling strength is decreased from 1 to 0 (cf. [2]). When, for example, $a = 2$, the synchronous phase in GCM is maintained until $\bar{c} = 0.5$, where it destabilizes and is substituted by the so called 'glassy phase'. In Kaneko's terminology, 'glassy' means that the final attractor is sensitive to the initial state of the maps, and thus a multiplicity of attractors is to be found in this phase for the same parameters value. For $\bar{c} = 0.33$, an ordered phase sets in: The sensitivity to the initial conditions disappears and the elements group together in only 2 or 3 different clusters. A narrow intermittent band in $0.21 < \bar{c} < 0.25$ precedes the turbulent phase, in which the number of clusters in all the attractors is of order $O(N)$.

We first examine the possibility of full mutual synchronization in RCM. Such full synchronization takes place in GCM when the coupling strength exceeds a critical value [3]. In the fully synchronized (coherent) regime the states of all maps in GCM are identical. Our analysis reveals that such exact synchronization does not occur in RCM. However, at sufficiently high coupling intensities, all elements move together in a single compact cloud (a fuzzy cluster), so that the typical distances between their trajectories remain below $|x^i(t) - x^j(t)| \sim 10^{-8}$ (this is the single precision for real numbers in our com-

puter). The fuzzy synchronous phase is maintained for a certain range of values of the coupling strength ϵ , and then a sudden transition to an asynchronous state (see the discussion below) is observed. Fig. 1 shows how this transition proceeds for a randomly chosen network with $\epsilon = 0.8$ and $N = 50$ elements. For comparison, we show in the same figure the respective behaviour of GCM. While for GCM the turbulent-ordered-glassy-synchronous sequence of phases is clearly seen when ϵ decreases, only the synchronization breakdown for RCM is apparent.

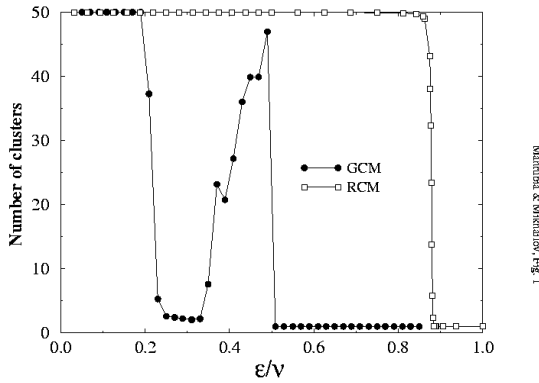


FIG. 1. Numbers of clusters as functions of the coupling strength ϵ for RCM of size $N = 50$ and connectivity $\epsilon = 0.8$ and for GCM ($\epsilon = 1$) of size $N = 50$. In the RCM case, two elements i and j are considered to belong to the same cluster if $|x^i(t) - x^j(t)| < 10^{-8}$. In the GCM case, two elements belong to the same cluster if their states are identical.

We have studied how the synchronization threshold in RCM depends on the mean connectivity of the network and on its size N . We accept that the elements in a given network are synchronized if the average distance d between pairs of elements during an interval t is smaller than 10^{-8} , after a transient is discarded, that is

$$d = \frac{1}{N(N-1)t} \sum_{h \neq j} \sum_{i \neq j} |x^i(t) - x^j(t)| < 10^{-8} : (3)$$

The simulations begin at a value of $\epsilon < \epsilon_c$ which is step-wise increased in amounts 10^{-3} until the condition (3) is fulfilled. We have also observed that immediately prior to the synchronization transition, the distance d undergoes a sharp cutoff and afterwards stabilizes around small values which depend on the system size (d is in the synchronous phase a decreasing function of N). In Fig. 2 the distance to the synchronization threshold of GCM is shown as a function of the network size when the connectivity is kept constant ($\epsilon = 0.9$). Numerically, we obtain

$$d_{GCM} \propto \frac{1}{N} : (4)$$

Large open circles are averages over 10 to 30 independent graphs, and are represented together with the dispersion

$$d(N) = \frac{\sqrt{\frac{1}{N} \sum_j (d_j(N) - \langle d(N) \rangle)^2}}{\langle d(N) \rangle} \quad \#_{1=2}$$

in the thresholds (error bars). The index j stands for different networks formed by the same number of elements N , while $\langle d(N) \rangle$ is the average value for each size. Small solid circles represent the synchronization threshold for each of these graphs. The error in the determination of ϵ_c for each network is 10^{-3} . The solid line in the main plot has slope $-1=2$.

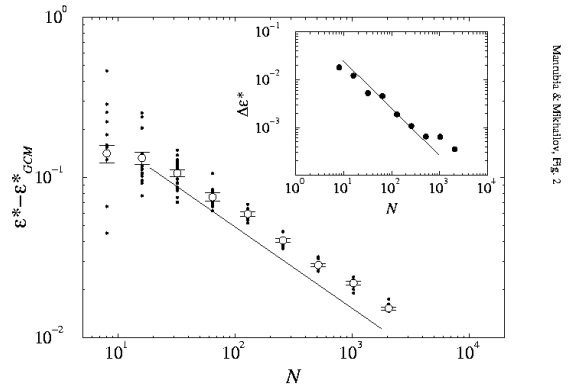


FIG. 2. Dependence of the synchronization threshold d on the network size N . The open circles correspond to average values of the critical coupling intensity ϵ_c for networks of sizes ranging from $N = 2^3$ to 2^{11} with the same connectivity $\epsilon = 0.9$. The solid line has slope $-1=2$. In the insert we show the dispersion in the values of ϵ_c as a function of the system size. The solid line has slope -1 . In this case, $a = 2$ and thus $d_{GCM} = 0.5$.

As larger networks are considered, the dispersion $d(N)$ in the synchronization thresholds for different networks with the same connectivity becomes smaller (insert). Our numerical results point to a dependence of the form $d \propto N^{-1}$. The fact that the dispersion in the values of ϵ_c tends to zero in the limit $N \rightarrow \infty$ for a fixed ϵ indicates that RCM are characterized by self-averaging quantities. In view of these results, the RCM should be well described by a mean-field approximation, thus by GCM, in the limit $N \rightarrow \infty$. In fact, the numerical simulations agree with this picture. In the opposite limit, when the number of elements in the system is small ($N \rightarrow O(1)$), the threshold at which the group first synchronizes is very sensitive to the particular way the maps are connected, as can be already seen for $N = 64$ in Fig. 2 (see also the Appendix). Fig. 3 depicts the synchronization threshold for systems with $N = 50$ and $N = 500$. Every point corresponds to a fixed network

with connectivity given in the x axes and the critical value in the y axes.

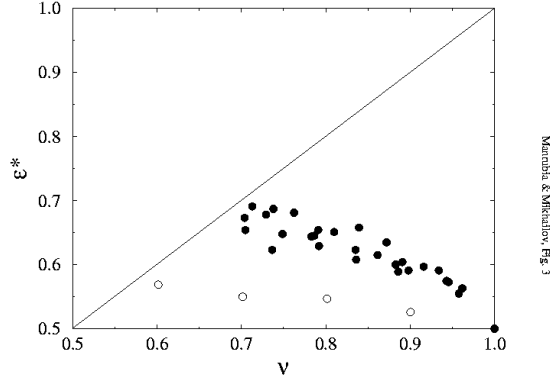


FIG. 3. Threshold to synchronization. Small solid circles are critical thresholds for systems of size $N = 50$ and big open ones correspond to $N = 500$. We restrict ourselves to values $\gamma = 0.3$, as discussed in the main text. The line $\epsilon^* = v$ is the stability threshold for GCM, and acts as a lower boundary for RCM.

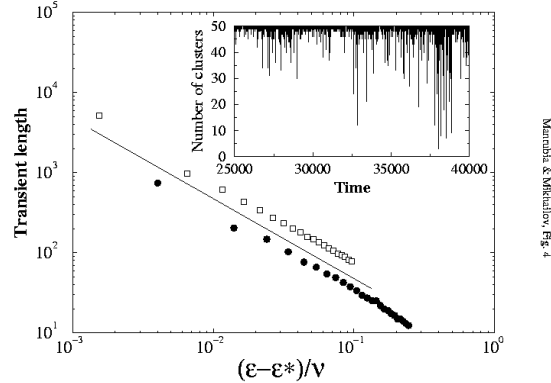


FIG. 4. Divergence in the transient time t_c when approaching the critical point for a randomly chosen network with $N = 50$ and $\gamma = 0.3$ (squares) and for the GCM of the same size (filled circles). The solid line indicates the divergence law with $\alpha = 1$. The inset displays the number of clusters as function of time for the RCM at $\gamma = 0.7$.

The synchronization threshold for GCM has previously been exactly determined [2]. When $N \rightarrow \infty$ it is given by the condition $\epsilon^* = \epsilon_{GCM}$ where the critical coupling is obtained from $\lambda + \log(1 - \epsilon_{GCM}) < 0$ and λ is the Lyapunov exponent of the single logistic map. It can be expected that the synchronization threshold for RCM approaches the limit $\epsilon^* = \epsilon_{GCM}$ when $N \rightarrow \infty$, for any value of γ , and also when $N \rightarrow \infty$, and independently of γ , as has been discussed. It can be seen from the numerical results represented in Figs. 2 and 3 that the

value $\epsilon^* = 0.5$ (for $\gamma = 2$) yields indeed a lower estimate for the synchronization threshold in RCM.

The system falls into the synchronous phase after a transient of diverging length when approaching the synchronization threshold. Fig. 4 shows the dependence of the transient time t_c on the distance to that threshold. The insert shows the dynamics during a typical transient. We see that strong fluctuations (intermittency) are accompanying the convergence process. Representing the dependence of the transient time in the form $t_c / (\epsilon - \epsilon^*)^\alpha$; we find that the exponent $\alpha = 1$ is typical both for RCM and GCM. More precisely, a least squares fit to numerical data returns $\alpha_{GCM} = 0.997(3)$ and $\alpha_{RCM} = 0.982(3)$, and the critical threshold values to synchronization are $\epsilon_{GCM} = 0.5$ and $\epsilon_{RCM} = 0.87$ for the particular graph of Fig. 4.

Below the synchronization transition, the glassy phase is observed in GCM. The dynamical behavior of RCM in the region $\epsilon < \epsilon^*$ is investigated in the next section.

III. MUTUAL INFORMATION AND THE TWO ORDER PARAMETERS

We have used three different measures of correlations among elements to check if the phase with $\epsilon < \epsilon^*$ has still some intrinsic order. The first of them is the mutual information between two maps i and j , $I^{ij}(\epsilon)$. To define this quantity, we introduce a partition of the phase space of the logistic map in the following way. If the state of the chosen element i is $x^i(t) \geq 0$ then it will be assigned a value 1, and 0 if $x^i(t) < 0$. This generates a sequence of bits in a certain time interval $S_t^i = \{x_t^i\}_{t=0}^{t_0-1}$ which allows the calculation of the Boltzmann entropy for the i th map [19],

$$H^i(\epsilon) = - \sum_{S_t^i = 0;1} P(S_t^i) \ln P(S_t^i) \quad (5)$$

In a similar way we define the joint entropy for each pair of maps,

$$H^{ij}(\epsilon) = - \sum_{S_t^i = 0;1} \sum_{S_{t_0}^j = 0;1} P(S_t^i; S_{t_0}^j) \ln P(S_t^i; S_{t_0}^j) \quad (6)$$

and finally the mutual information for i and j is given by

$$I^{ij}(\epsilon) = H^i(\epsilon) + H^j(\epsilon) - H^{ij}(\epsilon) \quad (7)$$

The mutual information is a good measure of correlations, e.g. it achieves maximal values near critical points [20]. In a context closer to ours it has been shown to accurately discriminate among the different phases of GCM [21]. An interesting property of I^{ij} is that it is practically precision-independent, due to the rough coarse-graining of the dynamics.

As an illustration of the sensitivity of this measure, let us discuss which values of I^{ij} are expected in two

dynamically opposite regimes, i.e. for the synchronous and the turbulent phases. In the coherent (synchronous) phase where the states of all elements are identical, the sequences S_t^i are the same for all of them, therefore $H^i(\cdot) = H^j(\cdot)$. In addition, since the two chosen maps are visiting the same points, we have $H^{ij} = H^i$ and thus $I^{ij} = H^i$, reflecting the trivial nature of the correlations. When $a = 2$, because of the symmetry in the invariant measure of the logistic map for this parameter (and noting that the synchronized system is equivalent to the single map) the mutual information achieves its maximum value. In fact, under these conditions, $P(0) = P(1) = 1/2$, thus maximizing $H^i = \ln 2$ and also $I^{ij} = \ln 2$. For parameter values $a \neq 2$ the invariant measure is not symmetric around 0, $P(0) \neq P(1)$ and hence $I^{ij} < \ln 2$ typically. Nonetheless, as can be seen in Fig. 5, the synchronous state is clearly detected through this measure. In the turbulent phase (assuming that the elements behave independently and are not correlated) we will have again $H^i(\cdot) = H^j(\cdot)$, but now the joint probabilities factorize, $P(S_t^i; S_t^j) = P(S_t^i)P(S_t^j)$ and $H^{ij} = 2H^i$. In this phase we therefore expect $I^{ij} = 0$ irrespectively of the parameter a . In the intermediate cases, where some correlations are present, the mutual information should take values between the former two limits, $0 < I^{ij} < \ln 2$.

To determine the mean mutual information

$$h^{ij}_i = \frac{2}{N(N-1)} \sum_{hi < ji} I^{ij}_i \quad (8)$$

for a network with a given matrix T_{ij} ; we take an average of the mutual informations for all possible pairs $(i; j)$ for long enough sequences to ensure the stability of the probabilities (typically $t = 10^3 - 10^4$ after discarding a transient). Fig. 5 shows the typical computed dependences of the mean mutual information h^{ij}_i on the coupling strength ϵ/V for RCM in the cases $a = 2$; 1.8 ; and 1.6 , and GCM. At low coupling intensities, the mutual information is zero, indicating the absence of correlations in the turbulent phase. It starts then to increase and reaches a maximum. In GCM this maximum corresponds to the ordered phase. When the coupling intensity is further increased, the mutual information falls down (at the onset of the glassy phase for GCM) before it finally increases and reaches a stable high value in the synchronous state. The effect of a decreased connectivity translates into a shift of the phases to higher values of the coupling. For low enough ϵ/V , synchronization is no longer possible (see also Fig. 3).

Thus, though by direct counting of the number of clusters (Fig. 1) we could not see any ordering in RCM for $\epsilon/V < 0.4$; the present analysis based on the measure of the mutual information clearly shows that the networks have intrinsic dynamical organization also in this region.

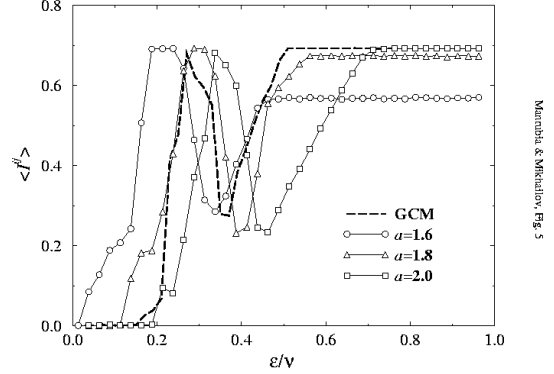


FIG. 5. Mean mutual information I^{ij} as function of the coupling intensity ϵ/V for a GCM ($\epsilon = 1$) of size $N = 200$ (dashed line) and three randomly chosen networks of the same size, connectivity $\epsilon = 0.8$ and values of a as shown. The sequences S_t^i were taken after discarding a transient of 10^3 steps. The GCM data is additionally averaged over 100 random initial conditions, and the RCM over 25 independent graphs.

Further characterization of different RCM phases is provided by two order parameters [5]. We examine all different $N(N-1)/2$ pairs of elements in the system and count how many of them are at a distance shorter than a fixed given precision δ . The first order parameter $r(\delta)$ is defined as

$$r(\delta) = \frac{2}{N(N-1)} \sum_{hi < ji} \mathbb{1}_{|x^i(t) - x^j(t)| < \delta} \quad (9)$$

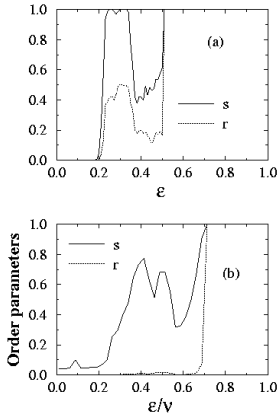
where $\mathbb{1}(x)$ is a step function, $\mathbb{1}(x) = 0$ for $x < 0$ and $\mathbb{1}(x) = 1$ for $x > 0$. The sum is taken over all possible ordered pairs $hi < ji$. The second order parameter $s(\delta)$ is given by the relative number of elements having at least one other element at a distance $d < \delta$.

In globally coupled systems the synchronization proceeds until all the elements in the same cluster asymptotically reach identical dynamical states. In this case, one can choose the highest available precision in the calculation of the two order parameters (in actual simulations it is limited by the computer precision). As we have already noted, this absolute synchronization does not occur in RCM. Instead, only clusters of elements having close dynamical states are formed here. Therefore the choice of the precision δ becomes important when networks are considered.

We have computed the order parameters as functions of the effective coupling strength ϵ/V for RCM and the respective GCM using varying precisions δ . It was found that the results for GCM only weakly depended on the precision in a wide interval $10^{-10} < \delta < 10^{-3}$. The curves shown in Fig. 6(a) for GCM have been calculated using $\delta = 10^{-6}$. We see that the order parameter r for GCM reaches, as should be expected, the value $r = 1$ in the fully synchronous (coherent) state at high coupling

intensities. However, a large relative number r of synchronous pairs is also found in this case at lower coupling intensities in the ordered phase. Moreover, the second order parameter s in this phase is close to 1 indicating that almost all elements belong to one of the synchronous clusters.

In contrast to globally coupled systems, dynamical clustering and synchronization in RCM is best resolved when an optimal small precision is employed. The plots shown for RCM in Fig. 6(b) have been therefore constructed for the optimal precision $\epsilon = 10^{-3}$. We see that in the region $\epsilon > \epsilon_c$; where fuzzy mutual synchronization is observed, both order parameters reach their maximal possible values, $r = s = 1$: Below the synchronization threshold, both order parameters rapidly decrease but then show a maximum. For small coupling intensities, the order parameters become very small (a somewhat larger initial level of s is explained by the fact that ϵ is larger here than in Fig. 6(a) and therefore a small number of pairs separated by the distance ϵ is found already in the turbulent phase, for the random independent distribution over the one-particle attractor).



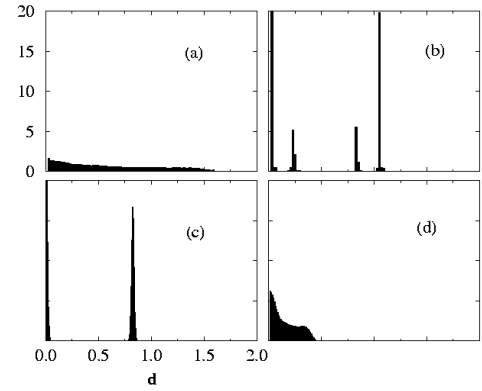
Marras & Mikulowicz Fig. 6

FIG. 6. Order parameters r (dotted lines) and s (solid lines) as functions of the coupling intensity ϵ for a GCM of size $N = 250$ (a) and for a randomly chosen network (the same as in Fig. 5) of size $N = 250$ and connectivity $\epsilon = 0.8$ (b). The employed precisions are $\epsilon_{\text{GCM}} = 10^{-6}$ and $\epsilon_{\text{RCM}} = 10^{-3}$. Averaging over 100 random initial conditions is additionally performed for GCM.

Thus, the behavior of the order parameters is again qualitatively similar in RCM and GCM. We can conclude that within a certain interval of coupling intensities, dynamical clustering of elements occurs in these systems. The difference is that, in the case of RCM, the clusters are fuzzy and can therefore be identified only when a sufficiently low precision is used. One further difference is that for RCM the order parameters do not fall down so sharply immediately below the synchronization threshold and a significant number of elements still has close neighbours in this region.

IV. DISTRIBUTIONS OVER PAIR DISTANCES AND DYNAMICAL CLUSTERS

Additional information about the structure of different phases in RCM is provided by histograms of distributions over pair distances. Such histograms are constructed by counting at a given time moment the numbers of pairs $(i; j)$ with distances $d_{ij} = |x_i - x_j|$ lying within subsequent small intervals d . Fig. 7 shows these normalized histograms for one fixed randomly chosen network with a large number of elements ($N = 1000$) at several coupling intensities. In the turbulent phase, a flat distribution corresponding to almost independent elements is found (Fig. 7(a)). When the coupling intensity is increased, some inhomogeneities start to develop in the distribution (the mutual information and the order parameters also begin here to increase). The peaks appearing later in the distributions indicate the onset of dynamical clustering (Fig. 7(b)). In the situation shown in Fig. 7(c) the system has two fuzzy clusters. When the coupling intensity is further increased, the cluster structure is destroyed and the distribution characterized by a broad maximum at zero distance between elements is formed (Fig. 7(d)). As the coupling intensity grows, this maximum gets increasingly narrow until the synchronous state is reached at $\epsilon = 1$.



Marras & Mikulowicz Fig. 7

FIG. 7. Normalized histograms of distributions over pair distances d_{ij} for different coupling intensities (a) $\epsilon = 0.1$, (b) $\epsilon = 0.25$, (c) $\epsilon = 0.35$, (d) $\epsilon = 0.45$ for a randomly chosen network of size $N = 1000$ with connectivity $\epsilon = 0.8$. The histograms are obtained by counting the numbers of pairs with the distances falling inside subsequent intervals of width $d = 0.01$ at a fixed time moment $t = 200$ after the transient. The vertical and horizontal axes have the same scales in all these histograms and stand for the probability density and for the distance between states, respectively.

The distributions over pair distances in Fig. 7 correspond to fixed time moments and therefore cannot tell us anything about dynamical properties of the clusters. To analyze the underlying dynamical behavior of the system, we have plotted in Fig. 8(a-d) the typical time evolutions

of the distance between two elements for the histograms displayed in Fig. 7(a-d).

In the turbulent phase (Fig. 7(a) and 8(a)) the pair distance evolves in an irregular way and shows large variations, as it can be expected for two independent logistic maps. At the beginning of the clustering phase (Fig. 7(b) and 8(b)), the elements tend to stay much closer (notice the change in the vertical scale) and weak aperiodic oscillations are observed.

For coupling intensities near the top value of the mutual information (Fig. 7(c) and 8(c)), the elements lock into periodic trajectories. Examining the trajectories of individual elements, we have seen in this case that all of them are now periodic, though different for different elements of the system. Thus, the system acquires rigid internal organization and falls into a state of frozen disorder. The pair distance between two elements in a cluster shows in this case purely periodic variation. The clusters are rigid and no exchanges among them are observed. Figures 7(b,c) represent two elements belonging to the same cluster. The distance between intercluster pairs shows analogous behaviour (i.e. weak aperiodic oscillations or periodic dynamics) although then the typical separations are of order $O(1)$.

An interesting dynamical behavior is observed for higher coupling intensities, preceding the synchronization transition (Fig. 7(d)). Now the elements alternate between short periods of partial synchronization and excursions away from the incipient cluster (Fig. 8(d), note the increase in the vertical scale). This form of behavior is in fact very reminiscent of on-off intermittency [15]. Such intermittency can explain the origin of the broad shoulder in the histogram of Fig. 7(d): It is formed by the elements that temporarily find themselves during a large excursion from the central cluster.

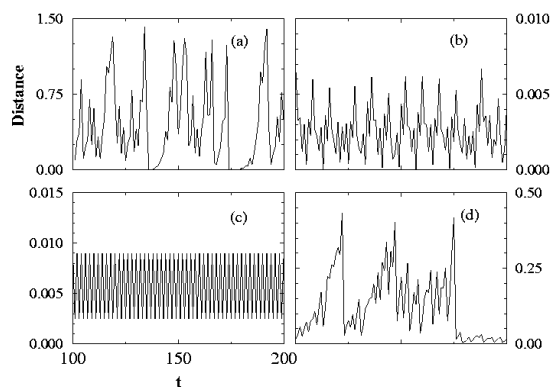


FIG. 8. Time evolution of the distance between a pair of elements in the same random network as in Fig. 7 for different coupling intensities (a) $\alpha = 0.1$, (b) $\alpha = 0.25$, (c) $\alpha = 0.35$, and (d) $\alpha = 0.45$: In cases (b) and (c) the elements belong to the same cluster.

The previous analysis has been also carried out for $\alpha = 1.8$. The above described picture is also obtained for this other value of the parameter in the logistic map and for corresponding coupling strenghts $\alpha = 0.1; 0.15; 0.25$ and 0.29 . This sequence is coherent with the different phases detected by the mean mutual information h^{ij} and represented in Fig. 5.

The formation of clusters with periodic dynamics has previously been observed in the ordered phase of globally coupled logistic maps [3]. As the coupling intensity is further increased, this ordered phase is replaced in this system by the glassy phase where the system has a large number of different attractors and its asymptotic dynamics strongly depend on the initial conditions. The glassy phase of GCM precedes the final transition to the fully synchronous coherent state.

An important result of our study is that the glassy behaviour was absent in the studied randomly coupled maps. When dynamical clustering was observed in this system, the cluster structure did not depend on the initial conditions and was completely determined by the architecture of the underlying graph. Moreover, the phase of dynamical clustering is separated in RCM from the synchronous phase by the region of intermittent regimes.

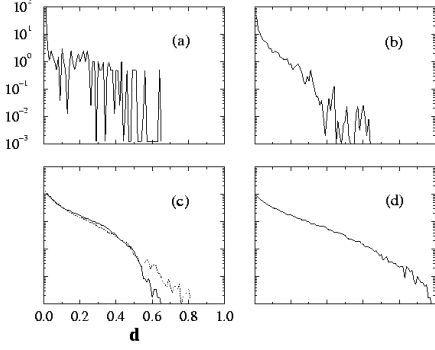
Our interpretation of this finding is that the quenched disorder introduced by randomly deleting some connections {transforming the GCM into RCM} is to a certain extent equivalent to the introduction of a small amount of dynamical noise (either multiplicative or additive) in a globally coupled system [22]. We have checked this conjecture by constructing the distributions over pair distances for GCM and RCM in the glassy and intermittent phases, respectively. Moreover, we have also computed similar distributions for GCM where an additive or a multiplicative noise have been included. The dynamical evolution of the noisy GCM is defined through

$$x^i(t+1) = (1 - \alpha) f(x^i(t)) + \frac{\alpha}{N} \sum_{j=1}^N f(x^j(t)) + g(x^i(t)); \quad (10)$$

where $g(x^i(t)) = r_i(t)x^i(t)$ in the multiplicative case and $g(x^i(t)) = r_i(t)$ in the additive case. We have used a small amplitude $\alpha = 10^{-3}$ for the noise, and $r_i(t)$ is a random number between -1 and 1 . It is chosen anew for each map at each time step.

Fig. 9(a) and (b) show in a logarithmic scale the histograms of distributions over pair distances in the glassy phase of the globally coupled logistic map under two different choices of the initial conditions for the same coupling intensity. We see that the resulting distributions are very different. Note that both distributions have been averaged over time, so that the peaks and irregularities in these figures reveal the persistent structure of the underlying attractors. Fig. 9(c) shows how these distributions are influenced by introducing into the GCM a weak additive (dashed line) or multiplicative (bold line) noise of

intensity $= 10^{-3}$ according to Eq. (7). The noises wash out the jagged structure of the distribution and, more importantly, make it independent of the initial conditions. The resulting distributions become then clearly similar to the respective distribution we obtain at the same coupling intensity for RCM, Fig. 9 (d).



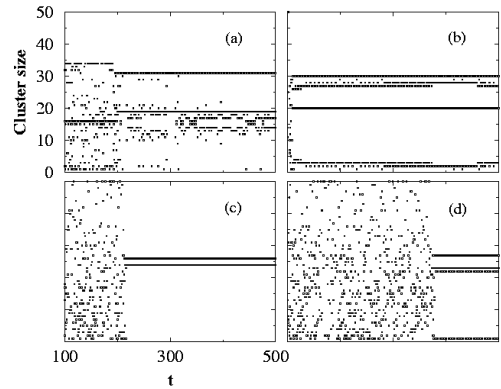
Murphy & Mészáros, Fig. 9

FIG. 9. Normalized histograms over pair distances for a GCM of size $N = 50$ and two different initial conditions (a,b), for the same GCM in the presence of an additive (dashed line) or multiplicative (bold line) noise of intensity $= 10^{-3}$ (c), and for a randomly chosen network of the same size with connectivity $= 0.8$ (d). The coupling intensity is $= 0.45$ in all these plots; time averaging is additionally performed.

We would like to emphasize that this parallelism between quenched disorder and dynamical noise might hold in the intermittent phase, but of course the mechanisms leading to the dynamical behaviour observed in other phases cannot be (at least solely) ascribed to noise. In the clustering phase, for instance, it should be clear that the fixed (though disordered) structure of the network plays the main role. In this sense, we have analysed the dynamical behaviour of the clusters by measuring in a fixed network how many elements belong to a certain cluster and how many clusters are formed at each time step. A cluster $C_m(i;t)$ for a given precision ϵ and at time t is formed by k_m elements, $m = 1; \dots; M$ such that all of them have at least another element of the cluster at a distance $d < \epsilon$, that is $d = |x_i(t) - x_j(t)| < \epsilon$, $\forall i$ and some $j \in C_m$ in order to say that also $i \in C_m$.

In Fig. 10 we represent the size of all clusters in a network with $N = 50$ elements as a function of time (for a fixed precision $\epsilon = 0.1$). Four different values of γ in the clustering phase have been chosen. In the first plot (Fig. 10 (a), $\gamma = 0.25$), the elements tend to cluster but the groups are still relatively unstable. A closer inspection of the clustering dynamics reveals that a group of 19 elements keeps stable in time, while another cluster containing the 31 remaining elements splits often in subgroups of sizes (17,14), (18,13) or (20,11) among others. If the coupling strength is increased, also the stability of

the clusters increases, and their average lifetime becomes longer. In Fig. 10 (b), for $\gamma = 0.28$ we observe that, in fact, larger and more stable clusters are formed. Now the elements are divided into a cluster with 20 elements and a second group with 30 that often splits into two subclusters with 27 and 3 elements, respectively. Some irregularities in the dynamics are also found. In the hard-locking phase for this network (Fig. 10 (c), $\gamma = 0.30$) two stable clusters with 24 and 26 elements are formed. As already discussed, the maps display periodic trajectories in this narrow parameter region. For a slightly larger $\gamma = 0.32$, in Fig. 10 (d), we see a first stable group with 27 elements and a second one with 23 including a weakly coupled map (which periodically leaves the cluster).



Murphy & Mészáros, Fig. 10

FIG. 10. Size and stability of synchronous groups in the clustering phase. The dynamical behaviour of a fixed network with $N = 50$ elements and $\gamma = 0.8$ is analysed for coupling strengths $\gamma = 0.25$ (a), $\gamma = 0.28$ (b), $\gamma = 0.3$ (c), and $\gamma = 0.32$ (d). The precision is in this case $\epsilon = 0.1$. Weakly coupled elements coexist with long-lived clusters which often split into smaller subgroups.

We have observed that the transient time required for the system to fall into the clustering phase increases with the increase of γ . At the same time, it is seen that elements have a trend to condense in a single group, as revealed by the presence of some time steps where the cluster size equals N . This is not found to happen at the beginning of the clustering phase, for values of $\gamma < 0.27$. Finally, for $\gamma = 0.35$ (in the network of Fig. 10) the maps do not form clusters any more and the intermittent phase begins.

V. PARTITIONS INTO DYNAMICAL CLUSTERS

In this section we more closely examine the structure of the dynamical clustering phase in RCM. In this phase, groups of maps moving together in a robust way and forming long-lived clusters have been observed. The emerging cluster structure is biased by the connection

patterns of the underlying network. To demonstrate this, we introduce relative connectivities that are defined below.

Let us suppose that at time t and with precision δ , our system separates into M clusters, $C_m(\delta; t)$, $m = 1; \dots; M$, each of which containing k_m elements. The relative connectivity inside a cluster m is then defined as

$$l_{eff}^m = \frac{1}{k_m(k_m - 1)} \sum_{i,j \in C_m; i \neq j} T_{ij}; \quad (11)$$

where the sum is taken over all pairs of elements belonging to this cluster. The relative connectivity between two different clusters l and n is given by

$$l_{eff}^{ln} = \frac{1}{k_l k_n} \sum_{i \in C_l; j \in C_n} T_{ij}; \quad (12)$$

Thus defined, the relative connectivities are equal to 1 if the characteristic connectivity inside a cluster or between two clusters are exactly the same as the average connectivity of the entire network. Positive deviations of the connectivity inside a cluster ($l_{eff}^m > 1$) indicate that this cluster contains elements which are more strongly connected than on the average. Respectively, when the relative connectivity between two clusters is decreased ($l_{eff}^{ln} < 1$), this shows that the elements belonging to these two separate clusters are less connected than on the average and vice versa.

We can also define the average intercluster relative connectivity of the entire network

$$l_{eff}^{inter} = \frac{1}{M(M-1)} \sum_{n,l=1; n \neq l}^M l_{eff}^{ln}; \quad (13)$$

and its average intracenter relative connectivity

$$l_{eff}^{intra} = \frac{1}{M} \sum_{m=1}^M l_{eff}^m; \quad (14)$$

To characterize the cluster structure of the partially ordered phase, we fix the coupling intensity and consider the state of the whole system at a given time moment. By varying the precision δ , we obtain a hierarchy of cluster partitions, as seen with different resolutions. For each resolution level, its relative connectivities are then calculated. Fig. 11 presents the emerging hierarchical structure of dynamical cluster partitions for a system of $N = 50$ elements with coupling strength $\gamma = 0.23$ at three different precisions δ . The numbers between brackets correspond to the number of elements in each particular cluster. The numbers inside the clusters are their relative connectivities and the numbers on the links between the clusters yield the relative connectivity between them. Though this pattern refers to a particular time moment (after a long transient), it remains fairly stable in time. We see that, as the precision δ is improved, the

clusters split into smaller subclusters, revealing a hierarchical tree-like structure [23]. It can also be observed in Fig. 11 that the relative connectivities inside a cluster exceed one, whereas the relative connectivities between the clusters are typically smaller than one. This indicates that the partition into dynamical clusters is biased by the pattern of connections in the underlying network, i.e. the elements belonging to a same cluster would generally have more connections inside this cluster than with the elements belonging to other dynamical clusters.

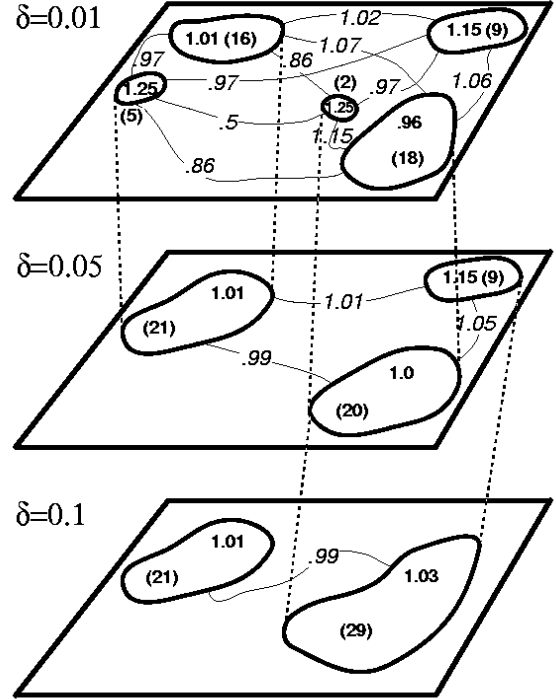


FIG. 11. Hierarchical structure of dynamical clusters for a randomly chosen network of size $N = 50$ with the connectivity $\gamma = 0.8$ at $\gamma = 0.23$.

To check more accurately this suggestion, we have calculated inter- and intracenter connectivities l_{eff}^{intra} and l_{eff}^{inter} for a larger system with $N = 250$ and $\gamma = 0.8$ at $\gamma = 0.3$ with the precision $\delta = 0.1$. These properties were averaged over 10^4 independent graphs. The average intracenter connectivity was in that case $l_{eff}^{intra} = 1.013(1)$; that is, slightly higher than numerically generated average connectivity, $h_{eff} = 1.0000(1)$. The average intercluster connectivity was $l_{eff}^{inter} = 0.987(1)$ and thus lying below h_{eff} . Figure 12 shows the normalized probability distribution over intracenter (solid line) and intercluster (dashed line) connectivities in the studied ensemble of 10^4 independently generated graphs. The maxima of the two distributions are slightly shifted. But, perhaps even more important, we see that the distribution of the intercluster connectivities is significantly

broad and has a wide shoulder extending towards lower connectivities.

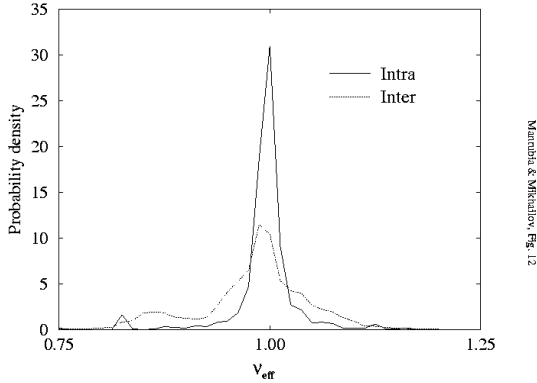


FIG. 12. Statistical distributions over intracluster (solid line) and intercluster (dashed line) effective connectivities in the clustering partitions in an ensemble of 10^4 independently generated random networks of size $N = 250$ with mean connectivity $\langle c \rangle = 0.8$ and coupling strength $\langle g \rangle = 0.3$. In this case, we have taken the precision $\epsilon = 0.1$.

V I. D I S C U S S I O N

Our numerical analysis reveals that mutual synchronization and dynamical clustering represent a typical and robust form of collective dynamics in random networks of coupled chaotic elements. The mutual synchronization remains possible when almost half of all potential connections between the elements are deleted and the dynamical clustering may be found even for the more sparsely connected networks. For very low connectivities, we have seen that the system could no longer synchronize and the dynamical clusters in the partially condensed phase became less stable, i.e. their lifetimes were getting shorter.

The different dynamical phases of RCM have been specified and compared with their counterparts in GCM. The essential differences have been noticed in the cluster structure and in the dynamics, as well as in the dependence on the initial conditions. A rich clustering structure, depending on the network architecture, was observed in RCM. The analog of the glassy phase of GCM was however not found in the investigated randomly coupled maps, i.e. we have not seen that the natural attractor depended on the initial conditions for any set of parameters. In this sense, the quenched disorder of the random network appears to play a role similar to that of noise in this phase. It might also be that the transition from synchronization to the intermittent phase in RCM would admit a characterization in terms of a blow out bifurcation [14], and that the intermittent phase that we observe immediately after the synchronous state be in fact a case of on-off intermittency. This picture would be consistent with our numerical results and with the fact that the

disorder in the network architecture destroys the degeneracy of the dynamical matrix in GCM [2] and generates a whole hierarchy of Lyapunov exponents.

Though our investigations were made only for networks formed by coupled logistic maps, similar results would probably hold for networks made of other chaotic maps or elements with continuous chaotic dynamics. Indeed, the behavior in globally coupled logistic maps strongly resembles what is found in various globally coupled populations of chaotic dynamical systems [5,8].

The systematic study of RCM implies the analysis of the behavior of the system under the change of four relevant parameters: The average connectivity $\langle c \rangle$, the coupling strength $\langle g \rangle$, the parameter of the individual map a , and the system size N . Our main interest in this study was to introduce Randomly Coupled Maps and to give some insights on the role of the network architecture in the dynamics. Hence, we have mainly investigated the two parameters $\langle c \rangle$ and N , and reanalysed the known phases for GCM when $\langle c \rangle$ varies from zero to unity. Many of our investigations were performed with control parameter $a = 2$ of the logistic map. This value is somewhat special, since at $a > 2$ the trajectories become infinite and the chaotic attractor disappears in a boundary crisis [24]. Other simulations for smaller values of the control parameter show a similar qualitative behaviour.

In our study, the networks were generated by independently choosing with a certain fixed probability the connection between any two elements. Thus constructed, the connection patterns are random, but statistically uniform. We have analysed systems with sizes ranging from a few elements to $N = 2^{11}$. Generally, the synchronization threshold depended not only on the system size and on the average connectivity, but also on the particular architecture of a chosen network. We have seen, however, that variations in the synchronization threshold for networks with the same mean connectivity became much weaker when the network size was increased, and that the distance to the mean field threshold given by GCM had the functional form $(\langle c \rangle_{GCM})' N^{-1/2}$. The existence of a universal synchronization threshold in such randomly generated networks in the limit $N \rightarrow \infty$ is thus expected. The statistical uniformity, introduced in this paper through the independent choice of individual connections, is a special feature that should not necessarily be present in complex networks. Natural networks may have various topological structures [25] which can also result from evolutionary processes [26,27]. It would be interesting to see how synchronization and the dynamical clustering phenomena are influenced by such structures.

We have found that the network architecture biases the partitions of the network into dynamical clusters and determines interactions between the clusters which lead to their collective dynamics. This puts forward the task of engineering the networks with the desired dynamical clustering properties. One can apparently design systems that would display an arbitrarily chosen partition

into several exactly synchronized clusters (see the Appendix). The collective dynamical behavior can represent an important practical function of a network. The evolution of a network, proceeding through random mutations, may then be guided towards the optimization of its collective dynamics. Indeed, examples of dynamical networks that evolve to reproduce given temporal melodies have already been constructed [28,29]. We want therefore to emphasize that the evolution of networks can also be steered to reach better synchronization properties or to approach a certain dynamical clustering structure.

Finally, we note that when the dynamical clustering is taking place, coherent clusters can be interpreted as super elements that form an emerging dynamical network of a higher structural level. Taking into account the large variety of clustering partitions and their sensitivity to the coupling intensity, RCM systems may thus be viewed as a living space that supports different dynamical (meta)networks and may retrieve a particular such network under appropriate changes of the control parameters.

ACKNOWLEDGMENTS

The authors acknowledge interesting discussions with Damiano H. Zanette. SCM gratefully acknowledges the support from the Alexander von Humboldt Foundation (Germany).

APPENDIX

It was earlier noted that the network architecture influences the critical coupling intensity at which synchronization first appears and favours certain preferred partitions of elements into dynamical clusters. In this Appendix we analyze the role of the network architecture in the dynamical clustering phenomena for small networks consisting of only $N = 5$ elements. If the network connectivity is fixed at $\alpha = 0.6$, there are just four such networks shown in Fig. 13. We have systematically investigated their synchronization properties for various values of the control parameter a of the logistic map in the interval from 1.42 to 2 with increment $\Delta a = 0.02$ and for the coupling intensity α in the interval from 0 to 1 with increment $\Delta \alpha = 0.01$. In this case we have considered that two maps are synchronized if they have exactly the same state. This is now licit because of the high degree of symmetry of the networks. The percent of parameter pairs leading to each of the possible clustering configurations is displayed in Table 1. In Fig. 13, elements with the same symbol synchronize (i.e. they form a cluster) with the higher probability. Different symbols stand for different clusters. The value of α at which the elements in each of the networks synchronize can take a wide spectrum of values. For instance, for $a = 1.6$ it

changes from 0.56 (case(A)) to 0.96 (case(B)) [30]. Moreover, we have found that α is a non-monotonic function of a , and can be even decreasing depending on the graph. Hence, if N is small, each network has to be treated independently (as in the example here analyzed).

We see that indeed in the majority of cases the clustering partition follows the pattern of connections in the graph. Moreover, some of the potential highly asymmetrical partitions have never been observed (like the partition into (1,5) (2,3) (4) for the graph A). This shows that the symmetry of connections inside a graph plays an important role in the dynamical clustering phenomena.

Looking at the graph A, we see that the dynamical equations of its elements are not changed under the relabeling $(1;2;3;4;5) \rightarrow (2;1;4;3;5)$, reflecting the symmetry with respect to permutations in the matrix T_{ij} for this graph. It seems highly plausible that synchronous clusters would generally be much easily formed by indistinguishable elements, defined as those whose dynamical equations are identical under permutations. This is the reason that allows synchronization to be of the hard locking (exact) type in this case. The numerical results shown in Table I support this statement.

Consider, for example, the situation in which the clusters (1,2), (3,4) and (5) have been formed in (A). Let us call $x^1(t) = x^2(t)$, $x^3(t) = x^4(t)$, y and $x^5(t) = z$ and write down the dynamic equations for the new 3-cluster system :

$$x(t+1) = (1 - \frac{5}{12}) f(x) + \frac{5}{12} f(y)$$

$$y(t+1) = (1 - \frac{5}{6}) f(y) + \frac{5}{12} (f(x) + f(z))$$

$$z(t+1) = (1 - \frac{5}{6}) f(z) + \frac{5}{6} f(y) \quad (A.1)$$

On the one hand, we do not observe any further (at least trivial) symmetry in these equations. On the other hand, the problem of global synchronization in our original graph has moved to the problem of synchronization of asymmetrically connected oscillators which moreover have different values for the coupling strength. According to this result, we believe that the problem of synchronization and clustering in RCM might also include asymmetrically connected networks and probably some cases of coupled systems with a distribution $P(\alpha)$ of values [13,12].

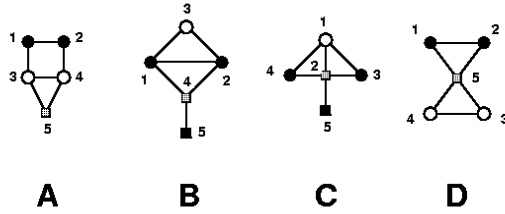


FIG. 13. Four different possible configurations of a network with $N = 5$ elements and $\epsilon = 0.6$. In each graph, favoured synchronizations are displayed using the same symbol.

[1] K. Kaneko, Phys. Rev. Lett. 63, 219 (1989).
[2] K. Kaneko, Physica D 41, 137 (1990).
[3] K. Kaneko, Physica D 75, 55 (1994); Physica D 55, 368 (1992).
[4] J.F. Heagy, T.L. Carroll, and L.M. Pecora, Phys. Rev. E 50, 1874 (1994).
[5] D.H. Zanette and A.S.Mikhailov, Phys. Rev. E 57, 276 (1998).
[6] Y. Kuramoto, Chemical Oscillations, Waves and Turbulence (Springer, Berlin 1984).
[7] D. Battogtokh, A. Preusser and A.S.Mikhailov, Physica D 106, 327 (1997).
[8] D.H. Zanette and A.S.Mikhailov, Phys. Rev. E 58, 1 (1998).
[9] P. Hadley and K. Wiesenfeld, Phys. Rev. Lett. 62, 1335 (1989).
[10] E. Niebur, H.G. Schuster, D.M. Kammen, and C. Koch, Phys. Rev. A 44, 6895 (1991).
[11] G. Caldarelli, P.G. Higgs and A.J. McKane, Jour. of theor. Biol. 193, 345 (1998).
[12] J.C. Stiller and G. Radons, Phys. Rev. E 58, 1789 (1998).
[13] D.H. Zanette, Europhys. Lett. 45, 424 (1999).
[14] J.C. Sommerer and E. Ott, Nature (London) 365, 136

(1993). E. Ott and J.C. Sommerer, Phys. Lett. A 188, 39 (1994); Yu. Maistrenko, T. Kapitaniak, and P. Szmanski, Phys. Rev. E 56, 6396 (1997).
[15] H. Fujisaka and T. Yamada, Prog. Theor. Phys. 74, 919 (1985); N.P. Latt, E.A. Spiegel, and C. Tresser, Phys. Rev. Lett. 70, 279 (1993).
[16] E. Ott, J.C. Sommerer, J.C. Alexander, I. Kan, and J.A. Yorke, Phys. Rev. Lett. 71, 4134 (1993).
[17] H. Fujisaka and T. Yamada, Prog. Theor. Phys. 69, 32 (1983).
[18] Yu. L. Maistrenko, V. L. Maistrenko, A. Popovich, and E. Mosekilde, Phys. Rev. E 57, 2713 (1998).
[19] The partition of the system has to be chosen in such a way that it is generating: There is a finite-to-one correspondence between infinite sequences and initial conditions. See for instance: S. Wiggins, Introduction to Applied Nonlinear Dynamical Systems and Chaos (Springer, Berlin, 1990).
[20] R.V. Sole, S.C. Manrubia, J. Bascompte, J. Delgado and B. Luque, Complexity 4, 13 (1996).
[21] J. Delgado and R.V. Sole, Phys. Rev. E 55, 2338 (1997).
[22] The effect of introducing different sources of disorder has been reported for instance in H. Bohr et al., Parallel Computing 12, 113 (1989); G. Abramson and D.H. Zanette, Phys. Rev. E 58, 4454 (1998); and in refs. [12] and [13].
[23] In Fig. 10, where the temporal behaviour of clusters is shown, only two or three clusters can often be seen. This however is explained by the low precision ($\epsilon = 0.1$) used in these plots. When the precision is increased, splitting of the clusters would be observed, similar to what is shown in Fig. 11.
[24] K.T. Alligood, T.D. Sauer, J.A. Yorke, Chaos, (Springer-Verlag, 1997).
[25] D.J.Watts and S.H. Strogatz, Nature 393, 440 (1998).
[26] S.A. Kauffman, The Origins of Order (Oxford University Press, 1993).
[27] K. Christensen, R. Donangelo, B. Koiller and K. Sneppen, Phys. Rev. Lett. 81, 2380 (1998).
[28] A.S.Mikhailov, J. Phys. A 21, L487 (1988).
[29] A.S.Mikhailov "Engineering of dynamical systems for pattern recognition and information processing", in Nonlinear Waves. Dynamics and Evolution, eds. A.V. Gaponov-Grekhov and M.I. Rabinovich (Springer, Berlin 1989) pp. 38-51.
[30] The value of ϵ is theoretically bounded by $\epsilon < 1$: For $\epsilon > 1$ divergencies in the values of x^i might be found. In practical terms, however, it is found that interactions among the elements prevent their states from attaining extremal values, and thus values of $\epsilon > 1$ can be used with caution.

TABLE I. Percent of realizations (%) for the clusterings shown and for each of the networks in Fig. 13.

Network	Clusters	%	Network	Clusters	%
A	(1,2,3,4,5)	5	B	(1,2,3,4,5)	1.5
	(1,2,5) (3,4)	2		(1,2,4) (3) (5)	1
	(1,2) (3,4,5)	1		(1,2) (3) (4) (5)	75
	(1,2) (3,4) (5)	59		(1,2,3,4) (5)	1
	turbulent	33		turbulent	21.5
C	(1,2,3,4,5)	2	D	(1,2,3,4,5)	4
	(1,2,3,4) (5)	1		(1,2,3,4) (5)	1
	(1,3,4) (2) (5)	17		(1,2) (3,4) (5)	57
	(1,3,4) (2,5)	0.5		(1) (2) (3,4) (5)	1.5
	(1,2) (3,4) (5)	0.5		(1,2) (3) (4) (5)	1.5
	(1) (2) (3,4) (5)	17		turbulent	35
	turbulent	62			